AGU ADVANCING EARTH AND SPACE SCIENCE

Geophysical Research Letters

RESEARCH LETTER
10.1029/2020GL089321

The Contribution of N^+ Ions to Earth's Polar Wind

Mei-Yun Lin[1], Raluca Ilie[1], and Alex Glocer[2]

[1]Department of Electrical and Computer Engineering, University of Illinois at Urbana-Champaign, Urbana, IL, USA, [2]NASA Goddard Space Flight Center, Greenbelt, MD, USA

Key Points:
- We developed a seven-ion polar wind model (7iPWOM), which solves for the outflowing N^+ ions
- N^+ ions are the second most abundant ionospheric species, up to 1,200 km
- The presence of N^+ ions improves the overall polar wind solution, when compared with observations

Correspondence to:
M.-Y. Lin,
mylin2@illinois.edu

Citation:
Lin, M.-Y., Ilie, R., & Glocer, A. (2020). The contribution of N^+ ions to Earth's polar wind. *Geophysical Research Letters*, *47*, e2020GL089321. https://doi.org/10.1029/2020GL089321

Received 16 JUN 2020
Accepted 29 AUG 2020
Accepted article online 2 SEP 2020

Abstract The escape of heavy ions from the Earth atmosphere is a consequence of energization and transport mechanisms, including photoionization, electron precipitation, ion-electron-neutral chemistry, and collisions. Numerous studies considered the outflow of O^+ ions only, but ignored the observational record of outflowing N^+. In spite of 12% mass difference, N^+ and O^+ ions have different ionization potentials, ionospheric chemistry, and scale heights. We expanded the Polar Wind Outflow Model (PWOM) to include N^+ and key molecular ions in the polar wind. We refer to this model expansion as the Seven Ion Polar Wind Outflow Model (7iPWOM), which involves expanded schemes for suprathermal electron production and ion-electron-neutral chemistry and collisions. Numerical experiments, designed to probe the influence of season, as well as that of solar conditions, suggest that N^+ is a significant ion species in the polar ionosphere and its presence largely improves the polar wind solution, as compared to observations.

Plain Language Summary Nitrogen is the most abundant element in the Earth's atmosphere. Around 78% N_2 and 21% O_2 form the air we breathe and expand into high-altitude atmosphere, the thermosphere, and eventually the ionosphere. The neutral molecules in the ionosphere are ionized by solar radiation, and some of them break up into atoms, and others become charged particles. The ionospheric ions with sufficient energy can flow out into space, and the abundances of these outflowing ionospheric ions highly impact the near-Earth plasma properties. Studies focused on outflowing O^+ ions have been conducted for several years. However, the contribution of N^+ ions to the outflow solution is still largely unknown due to the instrumental limitations. This letter addresses the transport and energization of ionospheric N^+ ions based on theoretical predictions, and examines the role of N^+ ions to the collision and chemistry in the topside ionosphere. This study shows that N^+ ions are important components in the high-altitude polar ionosphere and their abundances can be affected by the sunlight and seasonal variations.

1. Introduction

While the magnetospheric H^+ ions are sourced both in the solar wind and the ionosphere, the low charge state heavier ions, such as N^+ and O^+, can only come from the Earth's ionosphere through the process of ionospheric escape. The polar wind, first suggested by Axford (1968), represents an ambipolar outflow of thermal plasma from the high-latitude ionosphere to the low pressure magnetosphere. As it flows out, the polar wind undergoes several processes, from chemical to diffusion dominance, from subsonic to supersonic flow, and from collision dominated to collisionless, and the composition is changing from heavy to light ion dominance (Ganguli, 1996). The acceleration of ionospheric H^+ has been well explained by the "classical polar wind theory" (Banks, 1969; Banks & Holzer, 1968), where the ambipolar electric field continuously accelerates the ions and electrons upward, providing sufficient acceleration to allow them to overcome gravity. However, this theory does not include the necessary acceleration mechanisms, such as centrifugal acceleration (Delcourt et al., 1993), required to explain the acceleration of heavy ions and their subsequent escape from the ionosphere.

Since the discovery of O^+ ions in the magnetosphere (Shelley et al., 1972), the impact and contribution of O^+ ions in the Earth's magnetosphere-ionosphere system has been the subject of numerous studies (e.g., Glocer et al., 2009; Ilie et al., 2013, 2015; Kronberg et al., 2014; Schunk & Raitt, 1980; Schunk & Sojka, 1997). Heavy ions, which most studies considered to be O^+ only, control the mass and energy flow in the Earth's magnetosphere (Daglis et al., 1999; Hamilton et al., 1988; Winglee et al., 2002). The presence of the heavy ions in the Earth's magnetosphere can alter the wave propagation (Bashir & Ilie, 2018; Keika et al., 2011; Summers & Thorne, 2003; Summers et al., 2007), the mass loading of the magnetospheric plasma (Garcia et al., 2010; Nosé et al., 2005; Winglee et al., 2002; Wiltberger et al., 2010), the ring current formation and decay

(Daglis et al., 1999; Hamilton et al., 1988; Kistler et al., 1989; Liemohn et al., 1999), and the cross polar cap potential (CPCP) (Glocer et al., 2009; Ilie et al., 2013; Winglee et al., 2002). However, most of the past and current space missions lacked the possibility to distinguish N^+ from O^+, due to low mass resolution of available instrumentation. Therefore, the observational record of N^+ ions has been overlooked, and the transport and energization of ionospheric N^+ have not been considered by most studies (Ilie & Liemohn, 2016; Yamauchi, 2019). For example, the Ionosphere/Polar Wind Model (IPWM) assumes N^+ ions as stationary, while the density of N^+ ions is determined from chemical equilibrium because they are considered a minor ion species and, therefore, their dynamics are less important (Varney et al., 2014). In spite of only 12% mass difference between N^+ ($m = 14$) and O^+ ($m = 16$), as well as the same electric charge, N^+ and O^+ have different properties and manifest different behaviors (Ilie & Liemohn, 2016).

It is well established that O^+ is dominant ion up to 4,000–7,000 km (Yau et al., 2007, 2012). Albeit limited, several early NASA space missions reported on the presence and the importance of N^+ ions, in addition to that of O^+, in the terrestrial ionosphere. During undisturbed time, Polar Orbiting Geophysical Observatory (OGO2) and Explorer 31 observed significant amounts of N^+ ions in the ionosphere between 500 and 1,400 km above 60° latitude, and the number density of N^+ ions is generally 5% to 30% of O^+ ions (Brinton et al., 1968, 1971; Hoffman, 1967). Moreover, Ion Mass Spectrometer (IMS) on board NASA International Satellite for Ionospheric Studies (ISIS-2) (Hoffman, 1970) indicated that abundances of N^+ ions consistently varied together with those of O^+ ions at roughly 1 order of magnitude lower (Hoffman et al., 1974). In addition, N^+ seems to be a constant companion of outflowing O^+ during the storm time (Chappell et al., 1981), and its concentration varied with geomagnetic conditions (Craven et al., 1995). The abundance of N^+ ions in the ionosphere was reported to increase dramatically during the geomagnetic storm time (Hoffman et al., 1974). Ion flux measurements from the suprathermal mass spectrometer (SMS) on board the Akebono satellite (Whalen et al., 1990; Yau & Whalen, 1992) also showed that the ratio of $N^+/O^+ \sim 1$ in the dayside high-altitude (>1,000 km) polar (>70°) ionosphere during the main phase of a large storm.

Although several other observations have shown the importance of ionospheric N^+ ions in the ionosphere and magnetosphere, the mechanisms responsible for accelerating the ionospheric N^+ ions from eV to keV energies, as well as the relative abundance of N^+ ions in the high-altitude ionosphere, are still largely unknown. In the topside ionosphere, three possible mechanisms are known to produce and energize N^+ ions in the polar wind: photoionization, Suprathermal Electron (SE) impact, ion-neutral-electron collisions, and chemistry. The presence of SE can increase the electric potential drop and alter the ambipolar electric field (Glocer et al., 2012, 2017; Khazanov et al., 1997). Moreover, the reflected photoelectrons are considered to be a significant source of heat for the topside polar ionosphere (Varney et al., 2014). Ion-neutral-electron collision and chemistry also play a fundamental role in the dynamics and energetics of the polar wind (Schunk & Nagy, 2009). Ion-neutral-electron chemistry acts as a source of ions in the polar wind, while collisions are the main energy and momentum source for heavy ions upflow, as they can acquire sufficient energy from various collision mechanisms, including Coulomb collisions (ion-ion), nonresonant ion-neutral interactions, resonant charge exchange, and electron-neutral interactions (Yau et al., 1993). This letter presents the first study that addresses the role of N^+ ions in the overall polar wind outflow solution, based on a first principle numerical model, which is the Seven Ion Polar Wind Outflow Model (7iPWOM), developed from the Polar Wind Outflow Model (PWOM) (Glocer et al., 2009, 2012, 2017, 2018).

2. Seven Ion Polar Wind Outflow Model

To assess the role of N^+ ions to the overall outflow solution, the PWOM of Glocer et al. (2018) has been further developed to include N^+ ions in the ionospheric plasma. The PWOM solves for the supersonic ionospheric outflow solution, along high-latitude magnetic field lines, ranging from 250 km to a few Earth radii, and 65° latitude or above. The gyrotropic transport equations, including continuity, momentum, and energy equations, as well as the ambipolar electric field, derived from generalized Ohm's equation, are solved for electrons and three ion species, namely, H^+, He^+, and O^+. The number density of the neutral species, including O, H, O_2, N_2, and He, are derived from NRLMSISE-00 empirical model (Picone et al., 2002). The equation set (Gombosi & Nagy, 1989) is shown in the Equations 1–4:

$$\frac{\partial}{\partial t}(A\rho_i)+\frac{\partial}{\partial r}(A\rho_i u_i)=AS_i, \tag{1}$$

$$\frac{\partial}{\partial t}(A\rho_i u_i)+\frac{\partial}{\partial r}(A\rho_i u_i^2)+A\frac{\partial p_i}{\partial r}=A\rho_i\left(\frac{e}{m_i}E_\parallel-g\right)+A\frac{\delta M_i}{\delta t}+Au_iS_i, \tag{2}$$

$$\begin{aligned}\frac{\partial}{\partial t}\left(\frac{1}{2}A\rho_i u_i^2+\frac{1}{\gamma_i-1}Ap_i\right)+\frac{\partial}{\partial r}\left(\frac{1}{2}A\rho_i u_i^3+\frac{\gamma_i}{\gamma_i-1}Au_ip_i\right)=A\rho_i u_i\left(\frac{e}{m_i}E_\parallel-g\right)\\ +\frac{\partial}{\partial r}\left(A\kappa_i\frac{\partial T_i}{\partial r}\right)+A\frac{\delta E_i}{\delta_t}+Au_i\frac{\delta M_i}{\delta t}+\frac{1}{2}Au_i^2S_i,\end{aligned} \tag{3}$$

$$E_\parallel=-\frac{1}{en_e}\left[\frac{\partial}{\partial r}(p_e+\rho_e u_e^2)+\frac{A'}{A}\rho_e u_e^2\right]+\frac{1}{en_e}\left(\sum_i\frac{m_e}{m_i}\left[(u_e-u_i)S_i-\frac{\delta M_i}{\delta t}\right]+\frac{\delta M_e}{\delta t}\right). \tag{4}$$

The subscripts i and e refer to the ion and electron species, respectively. The parameter r represents the distance from the footpoint of the magnetic field line; m is the particle mass; ρ represents the mass density; A is the cross-sectional area of a magnetic flux tube, which varies inversely with the magnetic field strength; A' is the gradient of A; γ represents the specific heat ratio; κ denotes the heat conductivity; k is Boltzmann's constant; and g is the local gravitational acceleration. The following three terms will be further discussed: S_i represents the production or loss rates of a particular species, $\frac{\delta M}{\delta t}$ is the momentum exchange rate, and $\frac{\delta E}{\delta t}$ represents the energy exchange rate. Note that Equation 4 in Gombosi and Nagy (1989) was incorrect and the correct version is presented here. Since the PWOM assumes that the plasma is quasi-neutral, electrons are solved from the charge neutrality condition, and a steady state of electron velocity and energy assumption with the limitation of current conservation, as shown in the Equations 5–8:

$$n_e=\sum_i n_i, \tag{5}$$

$$u_e=\frac{1}{n_e}\left(\sum_i n_iu_i-\frac{j}{e}\right), \tag{6}$$

$$j=j_0\frac{A_0}{A}, \tag{7}$$

$$\begin{aligned}\rho_e\frac{\partial T_e}{\partial t}=(\gamma_e-1)\frac{m_e}{kA}\frac{\partial}{\partial r}\left(A\kappa_e\frac{\partial T_e}{\partial r}\right)-\rho_eu_e\frac{\partial T_e}{\partial r}\\ -T_e\left[S_e+\frac{\gamma_e-1}{A}\rho_e\frac{\partial}{\partial r}(Au_e)\right]+(\gamma_e-1)\frac{m_e}{k}\frac{\delta E_e}{\delta t}.\end{aligned} \tag{8}$$

Note that j represents the electric current density and the subscript 0 denotes the value for certain reference altitude, at which we assume that the cross-sectional area A is 1 cm^2 and corresponds to the lower boundary of the magnetic flux tube.

For the rest of the letter, we will refer to the PWOM of Glocer et al. (2018) as the three ion PWOM (3iPWOM), since it only solved for three ion species. The inclusion of N^+ as an additional ion species required the expansion of the PWOM from three to seven ions. The 7iPWOM, developed from the 3iPWOM, solves the same transport equations for electron and accounts for the contributions of seven ions, H^+, He^+, N^+, O^+, N_2^+, NO^+, and O_2^+. The inclusion of the molecular ion species, such as N_2^+, NO^+, and O_2^+ ions, is required in the 7iPWOM due to their significant abundances in the topside ionosphere, as well as their importance in the ionospheric photochemistry (Richards & Voglozin, 2011; Solomon, 2010). At this stage, the model does not track the field aligned transport of molecular ion species, and they are assumed to be stationary and having the same fixed temperature as the neutral species; however, the molecular ion densities are determined via chemical equilibrium. This assumption is established only in the quiet time when the molecular ion outflow is negligible, as there is no sufficient energization (Craven et al., 1985; Peterson et al., 1994; Yau et al., 1993). The neutrals number density are also obtained from NRLMSISE-00

Table 1
Updated Chemical Scheme in the 7iPWOM

Chemistry process	Reaction rate ($cm^3\ s^{-1}$)	Reference
$O + h\nu \rightarrow O^+ + e^-$	see text	
$O_2 + h\nu \rightarrow O^+ + O + e^-$	see text	
$He + h\nu \rightarrow He^+ + e^-$	see text	
$H + h\nu \rightarrow H^+ + e^-$	see text	
$O + e^* \rightarrow O^+ + 2e^-$	see text	
$O_2 + e^* \rightarrow O^+ + O + 2e^-$	see text	
$He + e^* \rightarrow He^+ + 2e^-$	see text	
$H + e^* \rightarrow H^+ + 2e^-$	see text	
$O^+ + N_2 \rightarrow N + NO^+$	1.2×10^{-12}	Schunk and Nagy (2009)
$O^+ + O_2 \rightarrow O_2^+ + O$	2.1×10^{-11}	Schunk and Nagy (2009)
$He^+ + O_2 \rightarrow O^+ + O + He$	9.7×10^{-10}	Schunk and Nagy (2009)
$He^+ + N_2 \rightarrow N_2^+ + He$	5.2×10^{-10}	Schunk and Nagy (2009)
$He^+ + N_2 \rightarrow N^+ + N + He$	7.8×10^{-10}	Schunk and Nagy (2009)
$H^+ + O \rightarrow H + O^+$	$2.2 \times 10^{-11} \times T_e^{0.5}$	Schunk and Nagy (2009)
$H + O^+ \rightarrow H^+ + O$	$2.5 \times 10^{-11} \times T_e^{0.5}$	Schunk and Nagy (2009)
$N + h\nu \rightarrow N^+ + e^-$	see text	
$N_2 + h\nu \rightarrow N^+ + N + e^-$	see text	
$N_2 + h\nu \rightarrow N_2^+ + e^-$	see text	
$O_2 + h\nu \rightarrow O_2^+ + e^-$	see text	
$NO + h\nu \rightarrow N^+ + O + e^-$	see text	
$NO + h\nu \rightarrow NO^+ + e^-$	see text	
$NO + h\nu \rightarrow O^+ + N + e^-$	see text	
$N_2 + e^* \rightarrow N_2^+ + 2e^-$	see text	
$O_2 + e^* \rightarrow O_2^+ + 2e^-$	see text	
$N_2 + e^* \rightarrow 2N^+ + 3e^-$	see text	
$N_2 + e^* \rightarrow N^+ + N + 2e^-$	see text	
$N^+ + O_2 \rightarrow NO^+ + O$	3.07×10^{-10}	Schunk and Nagy (2009)
$N^+ + O_2 \rightarrow O_2^+ + N$	2.32×10^{-10}	Schunk and Nagy (2009)
$N^+ + O_2 \rightarrow O^+ + NO$	4.6×10^{-11}	Schunk and Nagy (2009)
$N^+ + NO \rightarrow NO^+ + N$	2×10^{-11}	Lindinger et al. (1974)
$N^+ + O \rightarrow N + O^+$	2.2×10^{-12}	Richards and Voglozin (2011)
$N^+ + H \rightarrow N + H^+$	3.6×10^{-12}	Harada et al. (2010)
$N_2^+ + N \rightarrow N^+ + N_2$	10^{-11}	Richards and Voglozin (2011)
$N_2^+ + NO \rightarrow NO^+ + N_2$	4.1×10^{-10}	Schunk and Nagy (2009)
$N_2^+ + O \rightarrow NO^+ + N$	1.3×10^{-10}	Schunk and Nagy (2009)
$N_2^+ + O \rightarrow O^+ + N_2$	1.0×10^{-11}	Schunk and Nagy (2009)
$N_2^+ + O_2 \rightarrow O_2^+ + N_2$	5.0×10^{-11}	Schunk and Nagy (2009)
$O^+ + NO \rightarrow NO^+ + O$	8.0×10^{-13}	Schunk and Nagy (2009)
$N^+ + e^- \rightarrow N$	$3.6 \times 10^{-12} \times (\frac{250}{T_e})^{0.7}$	Schunk and Nagy (2009)
$N_2^+ + e^- \rightarrow N + N$	$2.2 \times 10^{-7} \times (\frac{300}{T_e})^{0.39}$	Schunk and Nagy (2009)
$NO^+ + e^- \rightarrow N + O$	$4.0 \times 10^{-7} \times (\frac{300}{T_e})^{0.5}$	Schunk and Nagy (2009)
$O_2^+ + e^- \rightarrow O + O$	$2.4 \times 10^{-7} \times (\frac{300}{T_e})^{0.7}$	Schunk and Nagy (2009)

Note. The complete chemical scheme adopted in the 7iPWOM (blue and black) versus in 3iPWOM (black only). Note that e^* represents the suprathermal electrons.

empirical model. However, the 7iPWOM includes two additional neutral species, NO and N. While the neutral N density is available from NRLMSISE-00 model, the neutral NO density is not, so it is approximated based on the chemical equilibrium value in the upper thermosphere (Bailey et al., 2002; Siskind et al., 2004). This is a reasonable assumption since the polar wind neutrals are considered as static species, meaning that there is no upward flux above 200 km. Therefore, the density of neutral NO only depends on the chemical source. In order to describe possible mechanisms that produce and energize N^+ ions in the polar wind, the 7iPWOM developed expanded schemes, including ionospheric chemistry and collision, as well as suprathermal electron production. In the following sections, we present a detailed description of the 7iPWOM, and the impact of these changes on the 3iPWOM.

2.1. Updated Chemical Scheme

In 7iPWOM, the production and loss of all ionospheric ion species contribute to the source term S_i in the Equations 1–3, implying that the change of the chemical scheme significantly impacts the outflow solution. The expanded chemical scheme includes 20 chemical reactions in 7iPWOM and is presented in Table 1. The SE production rate of outflowing ions are described in the following section. Other than the production of N^+ ions from the SE production, N^+ ions can be produced via dissociative charge transfer between He^+ and N_2 and between NN_2^+ and N. Conversely, N^+ ions can be lost through charge exchange with neutral atmosphere, such as with H, O_2, NO, and O, and the recombination with thermal electrons. The 7iPWOM expanded chemical scheme provides not only how N^+ and molecular ions are produced and lost, but also the additional ion production and loss sources for O^+ and H^+. For instance, O^+ ions can be produced via charge exchange between N^+ with neutral O_2 and O, and between N_2^+ and O, while O^+ ions are lost via charge exchange between O^+ and neutral NO.

2.2. Updated Collision Scheme

Collision processes are responsible for the change in momentum and energy (via the $\frac{\delta M}{\delta t}$ and $\frac{\delta E}{\delta t}$ terms in Equations 2 and 3). The momentum and energy exchange due to collision processes are approximated using the momentum transfer collision frequencies as the Chapman-Cowling collision integrals (Schunk & Nagy, 2009). That is, any velocity and temperature difference of between ion, neutral, or electron can cause the change of the momentum and energy transport equations. The 7iPWOM includes all the relevant collision parameters between ion-neutral-electron collisions, including Coulomb collisions, and resonant and nonresonant ion-neutral interactions. Therefore, since the 7iPWOM accounts for four additional ion species, namely, N^+, N_2^+, NO^+, and O_2^+, and two additional neutral species, NO and N, the contributions of collisions to the momentum and energy transport equations from all ions and neutrals in the 7iPWOM are expected to change.

2.3. Suprathermal Electron Production Rate

The SE production rates in the 7iPWOM are calculated based on the GLobal airglOW (GLOW) model (Solomon et al., 1988) solution, a two-stream electron transport model, which provides the photoelectron and secondary electron fluxes at various energies. The details of the suprathermal electron transport equation, and coupling with 3iPWOM are presented in Glocer et al. (2018). The 3iPWOM assumes that the SE impacts mostly the production of O^+. However, with the cross-sectional area of the neutral-electron collision provided (Gronoff, Simon Wedlund, Mertens, & Lillis, 2012; Gronoff, Simon Wedlund, Mertens, Barthlemy, et al., 2012), and the density of the relevant neutral species from NRLMSISE-00 model, the 7iPWOM has the capability to derive the production rate of each ion species. This expanded scheme can also quantify the SE production on the heavy ions, under different geomagnetic activity conditions.

3. Data

The observational data set used here comes from the Atmosphere Explorer (AE-C) and OGO-6 satellites, which covered from ~120–1,200 km altitude. The ion mass spectrometers on board the OGO-6 and AE-C were nearly identical (Hoegy et al., 1991), and all ion densities were either measured by a Bennet radio frequency ion mass spectrometer (Brinton et al., 1973; Taylor 1973) or a magnetic ion mass spectrometer (Hoffman et al., 1973). The AE-C, launched in December 1973, aimed to study the structure of thermosphere, especially how the photochemical processes govern the region (Richards & Voglozin, 2011). During the first year of operation, the latitude of perigee moved from about 68° north down to about 60° south, and the orbit became circular at ~390 km altitude. The OGO-6 was launched in June 1969 as one of the large observatory to study the interrelation of high-altitude atmospheric parameters during increased solar activity (Jackson & Vette, 1975). Although inclination of OGO-6 orbit was 82° north, the tilt of the dipole axis results in a wide range of latitude coverage (Taylor 1971).

The ion density data used in this letter are retrieved from Craven et al. (1995) and have been digitized to use. Each AE data point was averaged over 40 km altitude, all activity levels, and over 6 hr local time centered on noon or midnight. The data were divided into two ranges based on the invariant latitudes, as 60°–70° and 70°–90°, and averaged. The OGO-6 data was organized similarly as AE-C, and included all events for

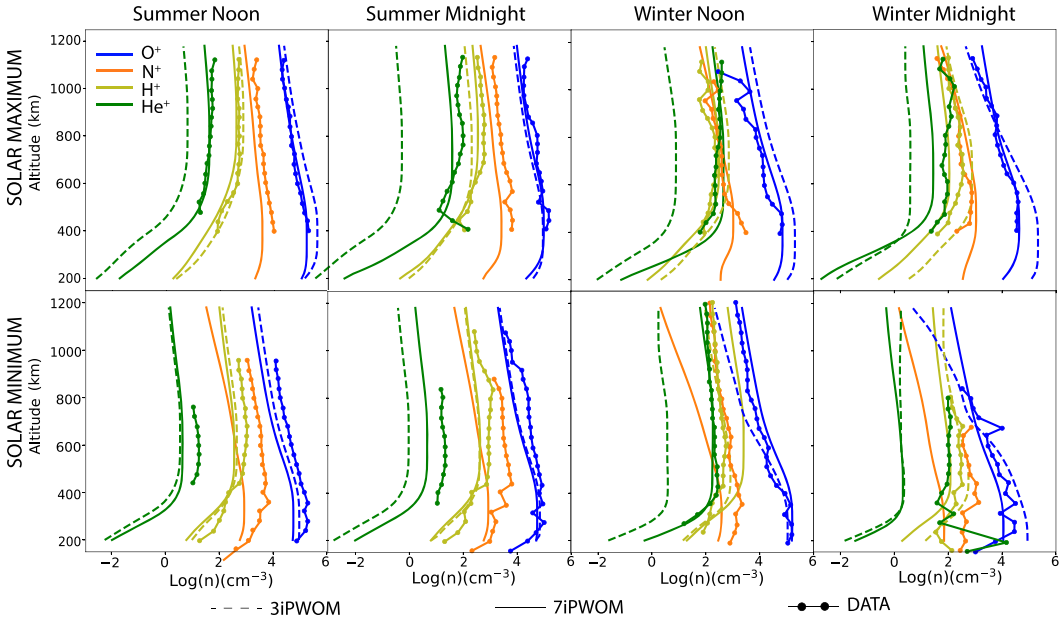

Figure 1. Polar wind densities for H^+ (light green line), He^+ (dark green line), O^+ (blue line), and N^+ (orange line) ions as predicted by 7iPWOM (solid line) and 3iPWOM (dashed line) under various solar and seasonal conditions. The dotted lines represent the data from AE-C (solar minimum) or OGO-6 (solar maximum).

which the F10.7 flux was larger than 120×10^{-22} WHz/m^2 during the peak solar activity of cycle 20, which was representative of solar maximum. The F10.7 index during the AE-C mission was generally ~70 to 100×10^{-22} WHz/m^2, and these data provide ion densities during solar minimum (Craven et al., 1995; Grebowsky et al., 1993).

4. Results

This letter presents an analysis of the relative contribution of the nitrogen ions to the overall outflow solutions based on eight different sets of numerical experiments, designed to probe the influence of season, as well as that of solar conditions. The 7iPWOM model results are validated using the data sets described in section 3.

4.1. Simulation Configuration

Figure 1 shows the simulation results from eight different sets of numerical experiments, designed to take advantage of data availability. All of the simulations use a time step of 10^{-3} s, with a field-aligned grid spacing of 20 km. The lower boundary of the 7iPWOM is at 200 km altitude, where the number density of ions is determined based on the chemical equilibrium assumption. The upper boundary is set around 8,000 km altitude and assumes to be a low-pressure region where the ion pressure decays with the ion scale height.

The 7iPWOM performance is validated using the data from OGO-6 satellites and AE-C satellite. The latitude locations for the footpoint of the field lines used for these eight simulations were selected to allow assessment of the effect of the solar zenith angle. To test the influence of solar conditions, we have run simulations for both solar maximum (top row) and solar minimum (bottom row) conditions. From left to right, each column presents the number density for H^+ (green line), He^+ (light green line), O^+ (blue line), and N^+ (orange line) transported along field lines, which the footpoints are located at noon and midnight during summer conditions and noon and midnight during winter conditions. The upward transport of these ions in the Earth's polar ionosphere (200–1,200 km) is solved for using both the 7iPWOM (solid line) and the 3iPWOM (dashed line), and comparison with the appropriate data (dotted line) from OGO-6 and AE-C for various solar flux and seasonal conditions is presented. Each simulation is initialized for 10 hours to achieve steady state. The nightside solutions are obtained via a 24 hr simulation, which allows a field line from the noon sector to

convect across the polar cap to the night sector for multiple times, with the convection velocity ($\vec{u} = \frac{\vec{E} \times \vec{B}}{B^2}$).

Note that as mentioned in section 3, each data point from AE-C and OGO-6 was averaged over 40 km altitude and over 6 hours local time. Therefore, the results from the 7iPWOM and the 3iPWOM are chosen to be the center of invariant latitude regions for the comparison of dayside solutions, and averaged from multiple simulations of magnetic field lines in neighbored locations to compare nightside solutions. For example, summer noon is represented by the steady-state solution of a single field line located in 80° latitude and 12 MLT, which is centered in the region of 70°–90° latitudes. Summer midnight is averaged by the convection result between one around 60°–65° latitude and 65°–70° latitude for the other, with the longitude close to 0 MLT. Note that the roots of simulated field lines are all located in the Earth's Northern Hemisphere, meaning that summer is denoted by 20 July and winter is set as 20 December.

4.2. The Role of N^+ in the Outflow Solution

Figure 1 shows that the 7iPWOM provides a reasonable prediction of the polar wind solutions in 200–1,200 km altitude, as compared with observations. For all geomagnetic conditions, the simulated ion number densities based on the 7iPWOM model are similar to the observed averaged OGO-6 or AE-C data. As expected, the O^+ ion is the most abundant ion species in the polar wind at these altitudes. However, the N^+ ion is the second most abundant ion for all geomagnetic conditions, confirming that N^+ ion is an important component of ionospheric outflow. Under most conditions, N^+ exceeds He^+ in concentration. Moreover, the abundance of N^+ ions consistently vary together with that of O^+ ions, being about 1 order magnitude lower for all seasons and solar conditions. All of these findings are in agreements with measurements from early missions, such as OGO-2 (Brinton et al., 1968), Explorer 31 (Hoffman, 1967, 1970), and ISIS-2 (Hoffman et al., 1974).

Figure 1 also shows that the 3iPWOM generally predicts higher number densities of O^+, and lower number density of He^+, as compared to the 7iPWOM solution. For instance, during solar maximum summer noon conditions, the number density of He^+ ions as predicted by 3iPWOM is 1 order of magnitude lower than the solution provided by the 7iPWOM, and the number density of O^+ ions predicted by the 7iPWOM is ~50% of that predicted by the 3iPWOM. This, together with the demonstrated improvement in data-model comparison, shows that the inclusion of N^+ ions in the polar wind model is important to ionospheric outflow modeling. The roles of ion-neutral-electron chemistry, collision, and SE production in the overall evolution of the polar wind solution when N^+ ions are present, are examined later in this letter.

4.3. Variations due to Seasons and Solar Flux

The variations in the N^+ number density due to changes in the solar flux are also presented in Figure 1. The abundances of both N^+ and O^+ ions decrease as the solar activity (represented by F10.7 index as a proxy in the model) decreases, but H^+ abundances are less affected. The 7iPWOM predicts higher heavy ion number densities in the sunlit and summer conditions, compared with dark and winter conditions. One of biggest improvement the 7iPWOM brings is the capability to capture the seasonal variation of He^+ ions, which at 1,000 km altitude in the winter season is 1 order magnitude larger than the summer, a feature the 3iPWOM does not capture. This significant seasonal variation of He^+ ions is due to the "winter helium bulge," which is an increase of helium neutral concentration at the exobase (Keating & Prior, 1968; Liu et al., 2014; Raitt et al., 1978).

During solar minimum, the 7iPWOM N^+ densities are lower compared to the AE-C data, especially above the 400 km altitude. A likely explanation is that the role of molecular ions becomes important during the solar minimum. Figure 2a1 shows the production rate of N^+ ions during the solar maximum summer noon, and the SE production is the most important reaction. This indicates that N^+ production is highly sensitive to solar activity. Therefore, the roles of the chemical reactions relevant to N^+ have been elevated during low solar flux activity, meaning that the productions of N^+ via charge transfer between He^+ and N_2 and, between N_2^+ and N, become important.

4.3.1. The Role of Chemistry

The chemical scheme plays a major role in determining the sources and losses of ionospheric plasma (Schunk & Nagy, 2009). Figure 2a1–a4 shows the production and loss of N^+ and O^+ ions via various chemical reactions as described in Table 1. In addition to production via SE production, heavy ions below 500 km

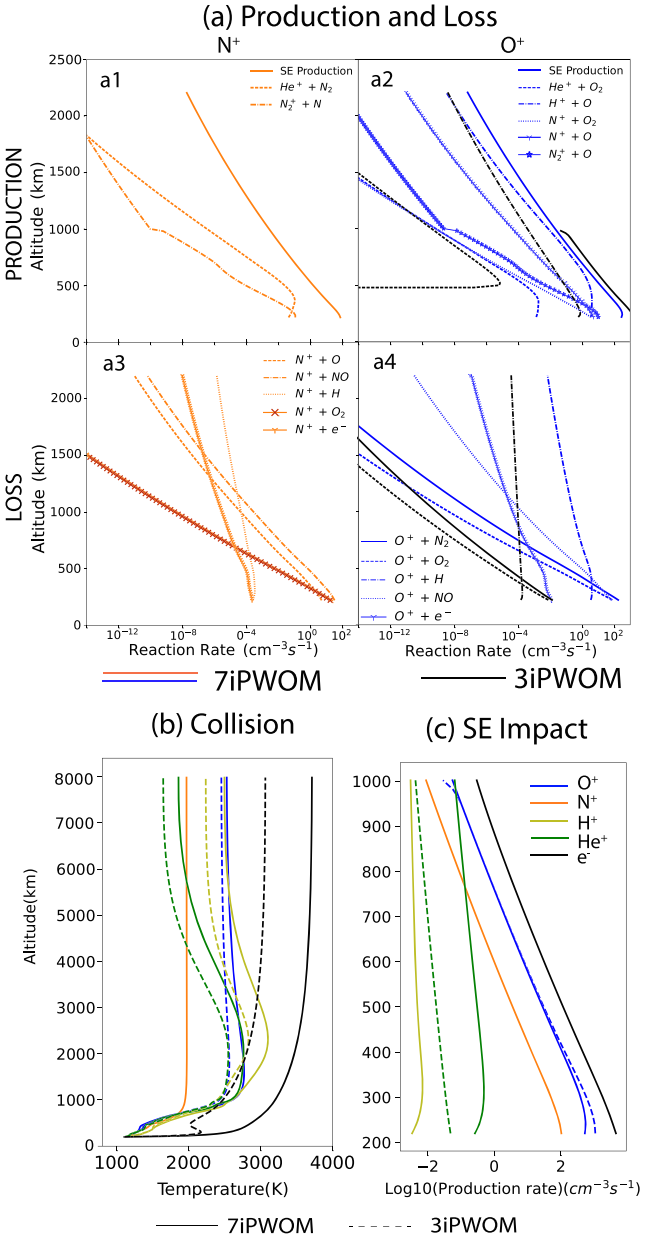

Figure 2. (a1–a4) Comparison of ion production and losses between 200 and 2,500 km, based on 3iPWOM (black) and 7iPWOM (colored lines); (b) altitude-dependent ion temperature profiles based on the 3iPWOM (dashed) versus 7iPWOM (solid) solutions; (c) ion production rate by SE in the 3iPWOM (dashed) versus 7iPWOM (solid).

can be produced by chemical reactions involving N^+, molecular ions, and neutral nitrogen-relevant species. Chemical reactions related to N^+ and molecular ions are important to produce heavy ions in the low altitude (Figure 2a1–a4), while as the altitude increases, the recombination reactions with e^- and the charge exchange of neutral H with heavy ions start to dominate, and can efficiently remove heavy ions from the polar wind. For example, the resonant charge exchange between H^+ and O is the major source for O^+ ions production (Banks & Kockarts, 1973; Yau et al., 2007). However, the charge exchange between N^+ and O can be the third important chemical reaction to produce O^+ ions and remove N^+. Figure 2a4 shows that the charge exchange between O^+ and NO, and the recombination of e^- and O^+ efficiently remove O^+ at low altitudes. During solar maximum summer noon conditions, the O^+ number density in the 7iPWOM chemical equilibrium solution of is 4.86×10^4 cm^{-3}, only 57% of that in the 3iPWOM solution, which is originally 1.17×10^5 cm^{-3}. On the other hand, the number density of N^+ and molecular ions are 5.73×10^3 cm^{-3} and 7.2×10^4 cm^{-3}. However, the total ion number density based on 7iPWOM (1.21×10^5 cm^{-3}) and 3iPWOM (1.17×10^5 cm^{-3}) are similar. The presence of N^+ in the ionospheric outflow largely redistributes the ion composition into different ion species and alters their altitude profile.

4.3.2. The Role of Collisions

Figure 2b shows the temperature profile of H^+, He^+, O^+, and N^+ ions during summer solar maximum from 3iPWOM and the 7iPWOM, respectively. In the collision-dominated region, the temperature of ions, mainly determined by the ion-neutral-electron collision, are identical for all the ion species. However, as the altitude goes up, the temperatures of N^+ and O^+ ions decrease as the velocity of H^+ increases, meaning that the temperature of O^+ and N^+ ions are tightly coupled with cold neutral species. Compared with the ion temperatures between the 3iPWOM and 7iPWOM, the 7iPWOM mostly predicted higher ion temperatures. The temperature of O^+, He^+, and H^+ ions increase due to the additional energy contribution from N^+ ions and updated neutral species. Furthermore, Figure 2b presents the temperature of N^+ ions in high altitude, which is lower than that of O^+ ions. This might be explained by the differences in the N^+-H and O^+-H collision, which are nonresonant and resonant collision, respectively. The energy transfer rate of the resonant collision is larger than that for nonresonant collisions, causing the temperature profile of N^+ to divert earlier than other ion species. Overall, the 7iPWOM solution accounts for the collisional contribution from N^+ ions and neutral species to the momentum and energy transfer, leading to different temperature profiles between the 3iPWOM and 7iPWOM.

4.3.3. The Role of Suprathermal Electron

The suprathermal electrons, even in small amounts, have been considered as an important energy source for the heavy ion outflow (Glocer et al., 2018; Khazanov et al., 1997). Figure 2a1–a2 shows a comparison of ion production and loss profiles based on the 7iPWOM and 3iPWOM solutions. It can be seen that the SE production is a major heavy ion production source in the polar wind. He^+ ions are only produced by the SE, and the 7iPWOM predicts He^+ abundances 1 order of magnitude more than the 3iPWOM does. The 3iPWOM uses a fixed but scaled He^+ production rate, while the 7iPWOM has an expanded scheme for SE production with altitude dependence. On the other hand, Figure 2c shows the SE production by the 7iPWOM and the

3iPWOM. The dashed blue line represents the production of O^+ ions due to SE production within the 3iPWOM, equal to the total SE production rate, and the solid blue line shows O^+ ions production rate due to SE production in the 7iPWOM. The 7iPWOM can account for the SE production rate as a function of altitude for all ion species, while the 3iPWOM assumes most of the SE production is linked to the production of O^+ ions only. This improvement of the 7iPWOM might be explained by this expanded scheme of SE production.

5. Summary

We have developed a seven-ion polar wind model (7iPWOM), as an extension of the 3iPWOM of Glocer et al. (2018), which solves for the transport of H^+, He^+, O^+, N^+, and e^- and includes three static minor ion species, NO^+, N_2^+ and O_2^+. Eight sets of numerical experiments have been conducted under various seasonal and solar conditions, and the 7iPWOM numerical model has been validated using data from the OGO-6 and AE-C satellites. Numerical simulations using the 7iPWOM suggest that (1) N^+ ions play an important role in the ionospheric outflow for all conditions, and the number density of N^+ ions is consistently 1 order magnitude less than O^+ ions at altitudes below 1,200 km; (2) the schemes of SE production, chemistry, and collision applied in the 7iPWOM improve the polar wind solution significantly, as it leads to an improved solution for He^+ ions and captures their seasonal variations; (3) the ion-electron-neutral chemistry and SE production control the production and loss of N^+, and the ion-electron-neutral collisions are responsible for their upward transport; and (4) N^+ ions are more likely to couple with cold neutral species, than the O^+ ions. This implies that the extra energy source provided by the inclusion of N^+ ions, such as through wave particle interactions, could have a profound influence on the upward transport of all polar wind ion species.

The 7iPWOM provides an updated view into the transport mechanisms behind the up-flowing of the major heavy ion species. Observations from Supra-Thermal Ion Composition Spectrometer (STICS) on board the Geotail indicates significant presence of N^+ and molecular ions in the magnetosphere, especially in the storm time (Christon et al., 2020); however, their transport is not quantified, nor understood, at this time. Therefore, knowledge of the differential transport and path of energization for the ionospheric heavy ions will help interpret observations and guide the development of instrumentation for future missions.

Acknowledgments
Work at University of Illinois at Urbana-Champaign was performed with financial support from AFOSR YIP Award No. AF FA 9550-18-1-0195, the NASA Grant 3004631577, and the NSF ICER Award No.1664078. The PWOM model has been included in the Space Weather Modeling Framework, which is available for download (at http://csem.engin.umich.edu/tools/swmf/downloads.php). Data generated for this study is available online (at https://doi.org/10.6084/m9.figshare.12457373).

References

Axford, W. I. (1968). The polar wind and the terrestrial helium budget. *Journal of Geophysical Research*, *73*(21), 6855–6859. https://doi.org/10.1029/JA073i021p06855

Bailey, S. M., Barth, C. A., & Solomon, S. C. (2002). A model of nitric oxide in the lower thermosphere. *Journal of Geophysical Research*, *107*(A8), SIA 22–1–SIA 22–12. https://doi.org/10.1029/2001JA000258

Banks, P. M. (1969). Plasma transport in the topside polar ionosphere. In G. Skovli (Ed.), *The Polar Ionosphere and Magnetospheric Processes* (pp. 193–208). New York: Gordon & Breach.

Banks, P. M., & Holzer, T. E. (1968). The polar wind. *Journal of Geophysical Research*, *73*, 6846–6854. https://doi.org/10.1029/JA073i021p06846

Banks, P. M., & Kockarts, G. (1973). Chapter 21—Physical processes in the topside ionosphere. In P. M. Banks & G. Kockarts (Eds.), *Aeronomy* (pp. 191–237). New York: Academic Press.

Bashir, M. F., & Ilie, R. (2018). A new N^+ band of electromagnetic ion cyclotron waves in multi-ion cold plasmas. *Geophysical Research Letters*, *45*, 10,150–10,159. https://doi.org/10.1029/2018GL080280

Brinton, H. C., Grebowsk, J. M., & Mayr, H. G. (1971). Altitude variation of ion composition in midlatitude trough region—Evidence for upward plasma flow. *Journal of Geophysical Research*, *76*(16), 3738–3745.

Brinton, H. C., Pharo, M. W. I., Rahman, N. K., & Taylor, H. A. J. (1968). Latitudinal variation of the composition of the topside ionosphere, first results of the OGO-2 ion spectrometer. Retrieved from https://ntrs.nasa.gov/citations/19680016284

Brinton, H. C., Scott, L. R., Pharo III, M. W., & Coulson, J. T. (1973). The Bennett ion-mass spectrometer on Atmosphere Explorer-C and -E. *Radio Science*, *8*(4), 323–332. https://doi.org/10.1029/RS008i004p00323

Chappell, C. R., Fields, S. A., Baugher, C. R., Hoffman, J. H., Hanson, W. B., Wright, W. W., et al. (1981). The retarding ion mass spectrometer on Dynamics Explorer-A. *Space Science Instrumentation*, *5*, 477–491.

Christon, S. P., Hamilton, D. C., Mitchell, D. G., Plane, J. M. C., & Nylund, S. R. (2020). Suprathermal magnetospheric atomic and molecular heavy ions at and near Earth, Jupiter, and Saturn: Observations and identification. *Journal of Geophysical Research: Space Physics*, *125*, e2019JA027271. https://doi.org/10.1029/2019JA027271

Craven, P. D., Comfort, R. H., Richards, P. G., & Grebowsky, J. M. (1995). Comparisons of modeled N^+, O^+, H^+, and He^+ in the midlatitude ionosphere with mean densities and temperatures from Atmosphere Explorer. *Journal of Geophysical Research*, *100*(A1), 257–268.

Craven, P. D., Olsen, R. C., Chappell, C. R., & Kakani, L. (1985). Observations of molecular ions in the Earth's magnetosphere. *Journal of Geophysical Research*, *90*(A8), 7599–7605.

Daglis, I. A., Thorne, R. M., Baumjohann, W., & Orsini, S. (1999). The terrestrial ring current: Origin, formation, and decay. *Reviews of Geophysics*, *37*, 407–438. https://doi.org/10.1029/1999RG900009

Delcourt, D. C., Sauvaud, J. A., & Moore, T. E. (1993). Polar wind ion dynamics in the magnetotail. *Journal of Geophysical Research*, *98*(A6), 9155. https://doi.org/10.1029/93JA00301

Ganguli, S. B. (1996). The polar wind. *Reviews of Geophysics*, *34*(3), 311–348.

Garcia, K. S., Merkin, V. G., & Hughes, W. J. (2010). Effects of nightside O^+ outflow on magnetospheric dynamics: Results of multifluid MHD modeling. *Journal of Geophysical Research*, *115*, A00J09. https://doi.org/10.1029/2010JA015730

Glocer, A., Khazanov, G., & Liemohn, M. (2017). Photoelectrons in the quiet polar wind. *Journal of Geophysical Research: Space Physics*, *122*, 6708–6726. https://doi.org/10.1002/2017JA024177

Glocer, A., Kitamura, N., Toth, G., & Gombosi, T. (2012). Modeling solar zenith angle effects on the polar wind. *Journal of Geophysical Research*, *117*, A04318. https://doi.org/10.1029/2011JA017136

Glocer, A., Tóth, G., Gombosi, T., & Welling, D. (2009). Modeling ionospheric outflows and their impact on the magnetosphere, initial results. *Journal of Geophysical Research*, *114*, A05216. https://doi.org/10.1029/2009JA014053

Glocer, A., Tóth, G., Ma, Y., Gombosi, T., Zhang, J.-C., & Kistler, L. M. (2009). Multifluid block-adaptive-tree solar wind roe-type upwind scheme: Magnetospheric composition and dynamics during geomagnetic storms—Initial results. *Journal of Geophysical Research*, *114*, A12203. https://doi.org/10.1029/2009JA014418

Glocer, A., Toth, G., & Fok, M.-C. (2018). Including kinetic ion effects in the coupled global ionospheric outflow solution. *Journal of Geophysical Research: Space Physics*, *123*, 2851–2871. https://doi.org/10.1002/2018JA025241

Gombosi, T. I., & Nagy, A. F. (1989). Time-dependent modeling of field-aligned current-generated ion transients in the polar wind. *Journal of Geophysical Research*, *94*, 359–369. https://doi.org/10.1029/JA094iA01p00359

Grebowsky, J. M., Hoegy, W. R., & Chen, T. C. (1993). High latitude field aligned light ion flows in the topside ionosphere deduced from ion composition and plasma temperatures. *Journal of Atmospheric and Terrestrial Physics*, *55*(11), 1605–1617. https://doi.org/10.1016/0021-9169(93)90137-N

Gronoff, G., Simon Wedlund, C., Mertens, C. J., Barthlemy, M., Lillis, R. J., & Witasse, O. (2012). Computing uncertainties in ionosphere-airglow models: II. the Martian airglow. *Journal of Geophysical Research*, *117*, A05309. https://doi.org/10.1029/2011JA017308

Gronoff, G., Simon Wedlund, C., Mertens, C. J., & Lillis, R. J. (2012). Computing uncertainties in ionosphere-airglow models: I. Electron flux and species production uncertainties for Mars. *Journal of Geophysical Research*, *117*, A04306. https://doi.org/10.1029/2011JA016930

Hamilton, D. C., Gloeckler, G., Ipavich, F. M., Wilken, B., & Stuedemann, W. (1988). Ring current development during the great geomagnetic storm of February 1986. *Journal of Geophysical Research*, *93*, 14,343–14,355. https://doi.org/10.1029/JA093iA12p14343

Harada, N., Herbst, E., & Wakelam, V. (2010). A new network for higher-temperature gas-phase chemistry. I. A preliminary study of accretion disks in active galactic nuclei. *The Astrophysical Journal*, *721*(2), 1570.

Hoegy, W. R., Grebowsky, J. M., & Brace, L. H. (1991). Ionospheric ion composition from satellite measurements made during 1970–1980: Altitude profiles. *Advances in Space Research*, *11*(10), 173–182.

Hoffman, J. H. (1967). Composition measurements of the topside ionosphere. *Science*, *155*(3760), 322–324. https://doi.org/10.1126/science.155.3760.322

Hoffman, J. H. (1970). Studies of the composition of the ionosphere with a magnetic deflection mass spectrometer. *International Journal of Mass Spectrometry and Ion Physics*, *4*, 315–322.

Hoffman, J. H., Dodson, W. H., Lippincott, C. R., & Hammack, H. D. (1974). Initial ion composition results from the Isis 2 satellite. *Journal of Geophysical Research*, *79*, 4246–4251.

Hoffman, J. H., Hanson, W. B., Lippincott, C. R., & Ferguson, E. E. (1973). The magnetic ion-mass spectrometer on Atmosphere Explorer. *Radio Science*, *8*(4), 315–322. https://doi.org/10.1029/RS008i004p00315

Ilie, R., & Liemohn, M. W. (2016). The outflow of ionospheric nitrogen ions: A possible tracer for the altitude-dependent transport and energization processes of ionospheric plasma. *Journal of Geophysical Research: Space Physics*, *121*, 9250–9255. https://doi.org/10.1002/2015JA022162

Ilie, R., Liemohn, M. W., Toth, G., Yu Ganushkina, N., & Daldorff, L. K. S. (2015). Assessing the role of oxygen on ring current formation and evolution through numerical experiments. *Journal of Geophysical Research: Space Physics*, *120*, 4656–4668. https://doi.org/10.1002/2015JA021157

Ilie, R., Skoug, R. M., Funsten, H. O., Liemohn, M. W., Bailey, J. J., & Gruntman, M. (2013). The impact of geocoronal density on ring current development. *Journal of Atmospheric and Solar-Terrestrial Physics*, *99*, 92–103. https://doi.org/10.1016/j.jastp.2012.03.010

Ilie, R., Skoug, R. M., Valek, P., Funsten, H. O., & Glocer, A. (2013). Global view of inner magnetosphere composition during storm time. *Journal of Geophysical Research: Space Physics*, *118*, 7074–7084. https://doi.org/10.1002/2012JA018468

Jackson, J. E., & Vette, J. I. (1975). The orbiting geophysical observatories. NASA SP-7601. NASA Special Publication, 7601.

Keating, G., & Prior, E. (1968). The winter helium bulge. *Space Research*, VIII, *8*, 982–992.

Keika, K., Brandt, P. C., Nosé, M., & Mitchell, D. G. (2011). Evolution of ring current ion energy spectra during the storm recovery phase: Implication for dominant ion loss processes. *Journal of Geophysical Research*, *116*, A00J20. https://doi.org/10.1029/2010JA015628

Khazanov, G. V., Liemohn, M. W., & Moore, T. E. (1997). Photoelectron effects on the self-consistent potential in the collisionless polar wind. *Journal of Geophysical Research*, *102*(A), 7509–7522.

Kistler, L. M., Ipavich, F. M., Hamilton, D. C., Gloeckler, G., Wilken, B., Kremser, G., & Stüdemann, W. (1989). Energy spectra of the major ion species in the ring current during geomagnetic storms. *Journal of Geophysical Research*, *94*(A4), 3579.

Kronberg, E. A., Ashour-Abdalla, M., Dandouras, I., Delcourt, D. C., Grigorenko, E. E., Kistler, L. M., et al. (2014). Circulation of heavy ions and their dynamical effects in the magnetosphere: Recent observations and models. *Space Science Reviews*, *184*(1-4), 173–235. https://doi.org/10.1007/s11214-014-0104-0

Liemohn, M. W., Kozyra, J. U., Jordanova, V. K., Khazanov, G. V., Thomsen, M. F., & Cayton, T. E. (1999). Analysis of early phase ring current recovery mechanisms during geomagnetic storms. *Geophysical Research Letters*, *26*, 2845–2848. https://doi.org/10.1029/1999GL900611

Lindinger, W., Fehsenfeld, F. C., Schmeltekopf, A. L., & Ferguson, E. E. (1974). Temperature dependence of some ionospheric ion-neutral reactions from 300–900 K. *Journal of Geophysical Research*, *79*(31), 4753–4756.

Liu, X., Wang, W., Thayer, J. P., Burns, A., Sutton, E., Solomon, S. C., et al. (2014). The winter helium bulge revisited. *Geophysical Research Letters*, *41*, 6603–6609. https://doi.org/10.1002/2014GL061471

Nosé, M., Taguchi, S., Hosokawa, K., Christon, S. P., McEntire, R. W., Moore, T. E., & Collier, M. R. (2005). Overwhelming O^+ contribution to the plasma sheet energy density during the October 2003 superstorm: Geotail/EPIC and IMAGE/LENA observations. *Journal of Geophysical Research*, *110*, A09S24. https://doi.org/10.1029/2004JA010930

Peterson, W. K., Abe, T., Fukunishi, H., Greffen, M. J., Hayakawa, H., Kasahara, Y., et al. (1994). On the sources of energization of molecular ions at ionospheric altitudes. *Journal of Geophysical Research*, *99*(A12), 23,257–23,274.
Picone, J. M., Hedin, A. E., Drob, D. P., & Aikin, A. C. (2002). NRLMSISE-00 empirical model of the atmosphere: Statistical comparisons and scientific issues. *Journal of Geophysical Research*, *107*(A12), SIA 15–1–SIA 15–16. https://doi.org/10.1029/2002JA009430
Raitt, W. J., Schunk, R. W., & Banks, P. M. (1978). Quantitative calculations of helium ion escape fluxes from the polar ionospheres. *Journal of Geophysical Research*, *83*(A12), 5617–5623. https://doi.org/10.1029/JA083iA12p05617
Richards, P. G., & Voglozin, D. (2011). Reexamination of ionospheric photochemistry. *Journal of Geophysical Research*, *116*, A08307. https://doi.org/10.1029/2011JA016613
Schunk, R., & Nagy, A. (2009). *Ionospheres* (Second). Cambridge: Cambridge University Press. https://doi.org/10.1017/CBO9780511635342
Schunk, R. W., & Raitt, W. J. (1980). Atomic nitrogen and oxygen ions in the daytime high-latitude F-region. *Journal of Geophysical Research*, *85*(NA3), 1255–1272.
Schunk, R. W., & Sojka, J. J. (1997). Global ionosphere-polar wind system during changing magnetic activity. *Journal of Geophysical Research*, *102*(A), 11,625–11,652.
Shelley, E. G., Johnson, R. G., & Sharp, R. D. (1972). Satellite observations of energetic heavy ions during a geomagnetic storm. *Journal of Geophysical Research*, *77*, 6104. https://doi.org/10.1029/JA077i031p06104
Siskind, D. E., Picone, J. M., Stevens, M. H., & Minschwaner, K. (2004). Middle and upper thermospheric odd nitrogen: 1. A new analysis of rocket data. *Journal of Geophysical Research*, *109*, A01303. https://doi.org/10.1029/2003JA009943
Solomon, S. C. (2010). Terrestrial ionosphere, *Heliophysics: Evolving solar activity and the climates of space and earth* (pp. 351–362). Cambridge: Cambridge University Press.
Solomon, S. C., Hays, P. B., & Abreu, V. J. (1988). The auroral 6300 Å emission: Observations and modeling. *Journal of Geophysical Research*, *93*(A9), 9867–9882. https://doi.org/10.1029/JA093iA09p09867
Summers, D., Ni, B., & Meredith, N. P. (2007). Timescales for radiation belt electron acceleration and loss due to resonant wave-particle interactions: 2. Evaluation for VLF chorus, elf hiss, and electromagnetic ion cyclotron waves. *Journal of Geophysical Research*, *112*, A04207. https://doi.org/10.1029/2006JA011993
Summers, D., & Thorne, R. M. (2003). Relativistic electron pitch-angle scattering by electromagnetic ion cyclotron waves during geomagnetic storms. *Journal of Geophysical Research*, *108*(A), 1143.
Taylor Jr., H. A. (1971). Observed solar geomagnetic control of the ionosphere-implications for reference ionospheres. *Advances in Space Research*, *12*, 1275–1290.
Taylor Jr., H. A. (1973). Parametric description of thermospheric ion composition results. *Journal of Geophysical Research*, *78*(1), 315–319. https://doi.org/10.1029/JA078i001p00315
Varney, R. H., Solomon, S. C., & Nicolls, M. J. (2014). Heating of the sunlit polar cap ionosphere by reflected photoelectrons. *Journal of Geophysical Research: Space Physics*, *119*, 8660–8684. https://doi.org/10.1002/2013JA019378
Whalen, B. A., Burrows, J. R., Yau, A. W., Budzinski, E. E., Pilon, A. M., Iwamoto, I., et al. (1990). The suprathermal ion mass spectrometer (SMS) onboard the Agebono (EXOS-D) satellite. *Journal of Geomagnetism and Geoelectricity*, *42*(4), 511–536.
Wiltberger, M., Lotko, W., Lyon, J. G., Damiano, P., & Merkin, V. (2010). Influence of cusp O^+ outflow on magnetotail dynamics in a multifluid MHD model of the magnetosphere. *Journal of Geophysical Research*, *115*, A00J05. https://doi.org/10.1029/2010JA015579
Winglee, R. M., Chua, D., Brittnacher, M., Parks, G. K., & Lu, G. (2002). Global impact of ionospheric outflows on the dynamics of the magnetosphere and cross-polar cap potential. *Journal of Geophysical Research*, *107*, 1237. https://doi.org/10.1029/2001JA000214
Yamauchi, M. (2019). Terrestrial ion escape and relevant circulation in space. *Annales Geophysicae*, *37*(6), 1197–1222. https://doi.org/10.5194/angeo-37-1197-2019
Yau, A. W., Abe, T., & Peterson, W. K. (2007). The polar wind: Recent observations. *Journal of Atmospheric and Solar-Terrestrial Physics*, *69*(16), 1936–1983. https://doi.org/10.1016/j.jastp.2007.08.010
Yau, A. W., Howarth, A., Peterson, W. K., & Abe, T. (2012). Transport of thermal-energy ionospheric oxygen (O^+) ions between the ionosphere and the plasma sheet and ring current at quiet times preceding magnetic storms. *Journal of Geophysical Research*, *117*, A07215. https://doi.org/10.1029/2012JA017803
Yau, A. W., & Whalen, B. A. (1992). Auroral ion composition during large magnetic storms. *Canadian Journal of Physics*, *70*(7), 500–509.
Yau, A. W., Whalen, B. A., Goodenough, C., Sagawa, E., & Mukai, T. (1993). EXOS D (Akebono) observations of molecular NO^+ and N_2^+ upflowing ions in the high-altitude auroral ionosphere. *Journal of Geophysical Research*, *98*(A7), 11,205–11,224.